

High chemical affinity increases the robustness of biochemical oscillations

Clara del Junco and Suriyanarayanan Vaikuntanathan

Department of Chemistry and The James Franck Institute, University of Chicago, Chicago, IL, 60637

Biochemical oscillations are ubiquitous in nature and allow organisms to properly time their biological functions. In this paper, we consider minimal Markov state models of non-equilibrium biochemical networks that support oscillations. We obtain analytical expressions for the coherence and period of oscillations in these networks. These quantities are expected to depend on all details of the transition rates in the Markov state model. However, our analytical calculations reveal that many of these details - specifically, the location and arrangement of the transition rates - become irrelevant to the coherence and period of oscillations in the limit where a high chemical affinity drives the system out of equilibrium. This theoretical prediction is confirmed by excellent agreement with numerical results. As a consequence, the coherence and period of oscillations can be robustly maintained in the presence of fluctuations in the irrelevant variables. While recent work has established that increasing energy consumption improves the coherence of oscillations, our findings suggest that it plays the additional role of making the coherence and the average period of oscillations robust to fluctuations in rates that can result from the noisy environment of the cell.

Many organisms possess circadian rhythms, “internal clocks” implemented as a series of chemical reactions that result in periodic oscillations in the concentrations of certain biomolecules over the course of a day [1, 2]. These oscillations are essential to regulate the timing of biological functions because they allow organisms to anticipate changes in daylight, thereby increasing the fitness of the organism [1, 3, 5]. Yet, each chemical reaction underlying a biochemical oscillator is a stochastic process, which leads to fluctuations in the period of oscillations and affects how accurately it can tell time. In addition to this inherent noise, other aspects of the heterogeneous environment inside a cell can increase the uncertainty in the clock’s period [6]. Understanding how biological organisms can robustly maintain the time scales of their clocks in the presence of these fluctuations is hence a central question [7–11], which we address in this letter. Our main result shows that in the limit that oscillations are driven by a high chemical affinity, the number of parameters that control their time scales can decrease dramatically. Oscillator time scales thus become insensitive to changes in many parameters, making them robust and tunable in the presence of fluctuations when the affinity - the nonequilibrium driving force - is high.

The model we use to derive our results (Fig. 1) is motivated by the fact that in the most general sense oscillators undergo (noisy) limit cycles. The model consists of N states connected in a ring that represents a projection of an oscillator’s average limit cycle. For instance, in the well-studied KaiABC oscillator of the cyanobacteria *S. elongatus*, these states would represent the different phosphorylation states of a population of KaiC proteins [4, 12, 13]. The system can hop between states with rates k_i^\pm , which could represent (de)phosphorylation rates. The source of oscillations is that the forward reaction rates in the KaiABC cycle are larger than the reverse rates. The rates in our model reproduce this asymmetry, creating a non-equilibrium steady state with a net clock-

wise current [14]. The chemical driving force responsible for the current can be quantified by the “affinity” of the network, $\mathcal{A} \equiv \log \prod_{i=1}^N k_i^+ / k_i^-$ [14]. In the case of KaiC, which is an ATPase, the affinity is provided by the highly exergonic hydrolysis of ATP [15]. If the system is initialized on a state i_0 in a network with a non-zero affinity, the probability associated with finding the system in any state will exhibit damped oscillations. The period of the oscillations reflects the average time taken by the system to traverse the ring and return to the state i_0 . The damping in the oscillations is an unavoidable consequence of the stochastic nature of the transitions. The ratio \mathcal{R} of the damping time to the oscillation time provides a figure of merit for the coherence of oscillations in the network [11, 16–18].

In principle, \mathcal{R} depends on all the details of the rates k_i^\pm in the network. However, in line with a large body of work that generically connects energy dissipation to accuracy in biophysical processes [20–25], it has been suggested that irrespective of these details the affinity bounds the coherence of biochemical oscillations [8, 17, 18, 26]. In particular, Barato and Seifert recently conjectured an upper bound on \mathcal{R} as a function of the number of states N and the affinity \mathcal{A} of the biochemical network [8]. The bound is saturated when the network is uniform; that is, when all of the counterclockwise (CCW) rates in the network are equal and all of the clockwise (CW) rates are equal. In this uniform limit, the bound tells us that only two variables (N and \mathcal{A}) determine \mathcal{R} . However, the bound is a weak constraint for non-uniform networks with arbitrary rates [8, 17] and hence it is unclear which variables control the time scales of the oscillator

in the presence of rate fluctuations. If the time scales depend sensitively on all of the rates in the network, then they might vary dramatically with any fluctuations. Conversely, if they depend on only a small subset of the variables, then they will be robust to any fluctuations

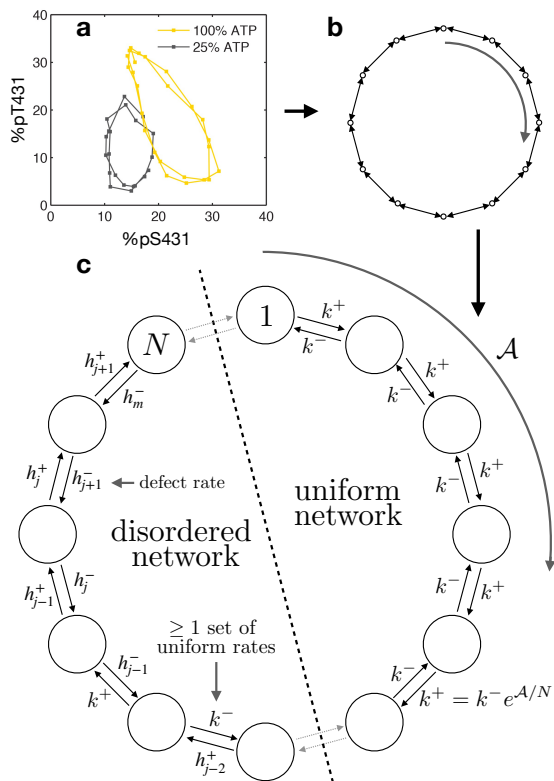


FIG. 1. A network of the kind studied in this paper as a model for a biochemical oscillator. (a) Biochemical oscillators trace a limit cycle in a high-dimensional state space of chemical concentrations. In this example of the KaiC oscillator, reprinted from Ref. [19], the axes represent the fraction of KaiC phosphorylated at each of two sites. (b) We approximate these limit cycles by projecting them down on to a single cycle of states. (c) Each node represents a state of the system, for instance, a phosphorylation state of KaiC. The system hops between states with rates k_j^\pm and is driven out of equilibrium by an affinity \mathcal{A} . This creates a net clockwise current, resulting in damped oscillations in the probability associated with finding the system in a particular state. We probe the dependence of the oscillation time scales on the rates of the network by adding ‘defect rates’ h_j^\pm to the uniform network, for which the time scales are known, and obtaining expressions for the coherence and period of oscillations in the disordered network. Our theory works in almost completely disordered networks, where only one rate is equal to the uniform value.

that do not affect this subset. We probe this question by obtaining analytical expressions for the time scales of Markov state models with non-uniform rates. As well as confirming the bound in Ref. 8, our main result, summarized in Eqs. 3 - 4, is that the number of coherent oscillations \mathcal{R} and the period of oscillations T , which in general depend on the magnitudes and locations of the all of the rates in the Markov state model, depend only on the single-site distribution of the rates when the affinity is sufficiently high. Our theory thus predicts that

\mathcal{R} and T are *predictable* using only the statistics of rate magnitudes and *robust* to any changes in the locations of the rates and any correlations between them. Numerical results confirm that with values of the affinity well within what is typically provided by ATP hydrolysis, our prediction is accurate even for networks where all of the rates take on random values that range over more than an order of magnitude. This confirms our prediction that the period and coherence of oscillations are controlled by a small set of parameters due to the presence of strongly non-equilibrium driving forces. As a consequence of our analytical theory, we find that high affinity significantly decreases the variance of \mathcal{R} and T over an ensemble of realizations of the rate disorder. This is our second main result. From a technical perspective, our results allow us to access values of the coherence and period in disordered regimes where \mathcal{R} is significantly smaller than the upper bound. From a biological perspective, our results suggest that as well as minimizing inherent fluctuations due to the stochasticity of the underlying processes [8–10, 17], a large energy budget has the additional, as-yet-unexplored advantage of making the coherence and period of oscillations robust and tunable even in the presence of the additional level of disorder in reaction rates.

An analytical expression for \mathcal{R} and T in disordered networks. As in Ref. 8, we compute \mathcal{R} from the ratio of the imaginary to real parts of the first non-zero eigenvalue (ϕ) of the transition rate matrix associated with the Markov state network. We also approximate the period of oscillations by $T \approx 2\pi/|\text{Im}[\phi]|$ and the correlation time by $\tau \approx -1/\text{Re}[\phi]$. Formally, T and τ depend on all the eigenvalues of the transition rate matrix. In the Supplementary Material (SM) [27], we show that ϕ captures the important features of T and τ .

The conjecture in Ref. 8 states that for a fixed affinity \mathcal{A} and number of states N , \mathcal{R} is bounded by

$$\mathcal{R} \leq \cot(\pi/N) \tanh[\mathcal{A}/(2N)] \equiv \mathcal{R}_0 \quad (1)$$

and that the bound is saturated in a uniform network, that is, when all of the rates in each direction are equal: $k_i^+ = k^+ = \exp(\mathcal{A}/N)k^-$ and $k_i^- = k^-$ for all i . The transition rate matrix $\mathbf{W}^{(0)}$ for the uniform network is given by

$$\mathbf{W}_{ji}^{(0)} = k^+ \delta_{i,j-1} + k^- \delta_{i,j+1} - (k^- + k^+) \delta_{i,j}. \quad (2)$$

$\mathbf{W}^{(0)}$ is a circulant matrix whose i th row is the top row shifted to the right by i columns [28]. Its eigenvalues are the discrete Fourier transform of the first row, giving $\phi^{(0)} = -(k^+ + k^-) + k^+ e^{-2\pi i/N} + k^- e^{2\pi i/N}$ from which \mathcal{R}_0 is immediately recovered. We begin from this known result in order to find how the addition of disorder changes ϕ and \mathcal{R} . We perturb the uniform network by adding some number $m \leq N-1$ of ‘defect rates’ denoted h_j^\pm as illustrated in Fig. 1; these could be due to some inherent asymmetry in the network (i.e. not all of the

reactions making up the cycle are the same), or due to fluctuations in variables such as concentration that affect reaction rates.

Rather than directly perturbing $\mathbf{W}^{(0)}$, which would restrict the defect rates to be close to the uniform rates, we recast the eigenvalue problem in terms of transfer matrices [29]. The transfer matrix formulation is useful for studying properties of systems with high degrees of translational symmetry and rapidly decaying spatial interactions and has been used to study localization in tight binding models [30] and neural networks [31], as well as dynamic [29] and structural phase transitions [32].

A detailed derivation is provided in SM section II [27]. The essential insight that it provides is as follows: in general, the new eigenvalue ϕ , and therefore \mathcal{R} , depends on all the details of the perturbed transition rate matrix. However, when the value of \mathcal{A}/N is large, significant simplifications are possible, leading to the following expression that depends only on the *values* of the defect rates and not their *relative locations*:

$$\begin{aligned} \phi &= \phi^{(0)} + \gamma & (3) \\ \gamma &= \frac{1}{m-N} \sum_{j=1}^m \log(\zeta'_j(\gamma)) + \frac{1}{2(m-N)^2} (\log(\zeta'_j(\gamma)))^2 & (4) \end{aligned}$$

An expression for $\zeta'_j(\gamma)$ is given in SI Eqs. 38 and 41 - it is a function only of γ , the j^{th} defect rate and of the uniform rates, and is independent of the rates at any other site. Eq. 4 is a nonlinear equation for γ which must be solved self-consistently. In SI Eq. 50, we provide a linear expansion. Our theoretical predictions in this paper are obtained numerically by searching for solutions to Eq. 4 near to the linear answer. Eq. 4 shows how the number of parameters that control the coherence and oscillation timescales decreases dramatically due to high chemical affinity.

We emphasize that this result is only valid if the affinity per state is sufficiently high (in practice, as we show below, $\mathcal{A}/N = 2$ is sufficient). Specifically, N/\mathcal{A} sets a length scale for correlations between defect rates, so that if $N/\mathcal{A} \ll 1$ even adjacent defect rates become decorrelated. ϕ generally depends on $\mathcal{O}(N)$ parameters: specifically, all the values and locations of the uniform and defect rates in the model. Eqs. 3 - 4 predicts that in this limit, ϕ depends on only a small, fixed number of parameters that does not scale with system size, namely, enough to specify the single-site probability distribution of the rates. As such, changes in the remaining, irrelevant parameters will not affect oscillator timescales - in other words, the oscillator is robust to these changes. As we demonstrate below, this implies that the timescales and coherence of oscillations can be maintained even when no two rates in the network have the same value.

Accurate theoretical predictions of coherence and period of oscillations with strong non-

equilibrium driving. To test the limits of Eq. 3, we compared it to the result of numerical diagonalization for networks of size $N = 100$ with up to 99 defect rates placed at random locations in the network. We considered networks with quenched disorder: we set all CCW rates to $k^- = h_j^- = 1$ and randomly selected the CW defect rates h_j^+ from a Gaussian probability distribution $P_G(\tilde{\sigma}, \mathcal{A}_0, N)$ with mean $k^+ = \exp(\mathcal{A}_0/N)$ and standard deviation $\sigma = \tilde{\sigma} \exp(\mathcal{A}_0/N)$, and with a lower cutoff at 0.1 so that we do not select rates that are very close to zero or negative. This prescription naturally allows the affinity to vary between networks - we show results for networks with fixed affinity in Fig. 3 of the SM [27] that confirm the bound in Eq. 1. Fig. 2 shows the importance of a high affinity (\mathcal{A}_0/N , the value of the affinity in the uniform network) for controlling \mathcal{R} and T . Our prediction from Eq. 3 improves with increasing \mathcal{A}_0/N : for $\mathcal{A}_0/N = 2$, Fig. 2 shows that Eq. 4 is accurate even when practically all of the rates in the network are random and $\langle \mathcal{R} \rangle$ is 40% less than the bound \mathcal{R}_0 [33]. (For comparison, the 24-state cycle of KaiC hexamer has $\mathcal{A}/N \gtrsim 10$ [12, 15, 34].)

While minimizing phase diffusion and thereby maximizing \mathcal{R} is a priority for a biochemical clock to keep time accurately, it is additionally important that T , the period of oscillations, be robust and tunable, for example in order to match with an external signal [5]. Our theory (Eq. 4) shows that T can be reliably controlled in the high affinity limit even in the presence of substantial disorder, and we also find that the spread of T values decreases significantly with increasing affinity. The excellent agreement of numerical results with our theoretical expression reveals a role for non-equilibrium driving that has, to the best of our knowledge, not been previously articulated: in addition to suppressing the uncertainty in the period due to the inherent stochasticity of the processes underlying oscillations, it also makes the oscillator timescales more robust by decoupling the rates of these processes.

The coherence and period of oscillations are robust to biologically relevant rate fluctuations. The “number of defect rates” is a convenient measure of disorder to use in the context of our theory, but is not clearly related to a biological scenario; in general we would expect all rates to fluctuate, for instance due to local fluctuations in the concentration of ATP, and that the disorder would be quantified by the size of the fluctuations. In Fig. 2 we showed that our perturbation theory can handle networks where effectively all of the rates fluctuate. In Fig. 3, we further investigate these fully disordered networks by showing how \mathcal{R} and T vary as a function of the spread of rates σ in a network with all CCW rates set to 1 and all CW rates drawn from the distribution $P_G(\tilde{\sigma}, \mathcal{A}_0, N)$ (defined in the previous section). All of our findings still hold: the prediction becomes more ac-

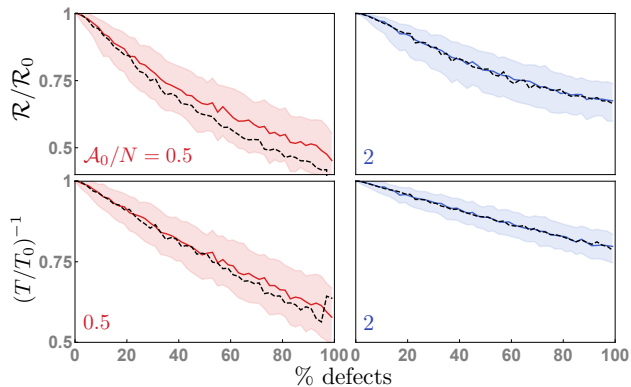


FIG. 2. Coherence \mathcal{R} and period T of an oscillator as a function of the percent of defect rates show that these values become more robust (spread of values decreases) and more predictable at high affinity. Results are for networks with $N = 100$ states. All CCW rates are set to 1. CW defect rates h_j^+ are drawn from a Gaussian distribution with mean $k^+ = \exp(\mathcal{A}_0/N)$ and standard deviation $0.4k^+$. Because the distributions of \mathcal{R} and T are asymmetric, we plot the median (solid line) \pm one quartile (shaded region) of the numerical values for 500 samples of defect rates. The dashed lines are the median theoretical predictions for 500 samples of defect rates. The affinity is allowed to vary. For $\mathcal{A}_0/N = 2$ (blue), our theory is accurate even when % defects ≈ 100 .

curate (Fig. 3a, b) and the spread of values of the time scales decreases (Fig. 3c) as the affinity \mathcal{A}_0 increases. In these networks the affinity naturally varies, and the average time scales are robust to these small variations.

Finally, we consider changes in the uniform rate, or \mathcal{A}_0/N . The bound in Eq. 1 implies that in a uniform network, the coherence \mathcal{R} becomes insensitive to changes in the affinity (Fig. 3c). However, it is not clear whether this will be the case in a disordered network. In Fig. 3, we show that even in a disordered network where $\mathcal{R} < \mathcal{R}_0$, the dependence of \mathcal{R} on \mathcal{A}_0/N vanishes smoothly for values of \mathcal{A}_0/N greater than ~ 5 . In this regime, our analytical results demonstrate how - due to non-equilibrium driving - the coherence is insensitive to large global fluctuations in the affinity that change the average rate k^+ as well as to small local fluctuations that cause the rates to fluctuate about k^+ .

Discussion and Conclusions. Biochemical oscillators, which can function as internal clocks, operate in noisy environments that can affect the ability of the clock to tell time accurately; yet somehow these oscillations continue with a well-defined period over long times. Here, we present analytical calculations supported by numerical results that show how a biochemical oscillator modeled as a Markov jump process on a ring of states (Fig. 1) can use high chemical affinity (for instance, in the form of ATP) to robustly maintain and tune its time scales even in the presence of a substantial amount of disorder. While previous work [8] has postulated an upper bound

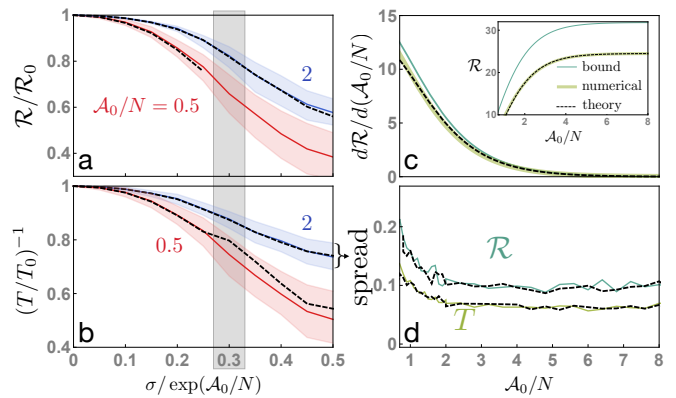


FIG. 3. (a) \mathcal{R} and (b) T for a totally disordered networks of size $N = 100$ as a function of the standard deviation of the distribution of defect rates. All CCW rates are set to 1. CW defect rates h_j^+ are drawn from a Gaussian distribution with mean $k^+ = \exp(\mathcal{A}_0/N)$ and standard deviation $\sigma = \bar{\sigma}k^+$. Results in right column are for networks with $\bar{\sigma} = 0.3$, indicated in gray. (c) The absolute value of \mathcal{R} as a function of \mathcal{A}_0/N plateaus in a totally disordered network with $\bar{\sigma} = 0.4$ as well as in uniform networks (given by the bound in Eq. 1). As a result, $d\mathcal{R}/d(\mathcal{A}_0/N)$ goes smoothly to zero with the same rate in the disordered and uniform networks, even though \mathcal{R} is far from the bound. (d) The ‘spread’, defined as the distance between the median ± 1 quartile of the data, as a function of the affinity. As predicted, it decreases with increasing affinity. Black dashed lines are theoretical predictions in all plots.

on the number of coherent oscillations that such a model can support in terms of the chemical affinity, the bound can be loose, and does not elucidate the dependence of the number of oscillations on the details of the rates in the network [8]. We close this gap by showing how in the limit of high affinity, the number of relevant variables controlling the coherence and time scales of oscillations dramatically decreases.

Specifically, we consider Markov state networks such as those in Fig. 1 and sample the rates from a probability distribution in order to mimic disorder in biological systems. Our analytical theory in Eqs. 3 - 4 reveals that in the limit of high affinity, the period of oscillations and the number of coherent oscillations depend only on the statistics of the probability distributions from which the rates are sampled. Factors such as the distance between the defect links or correlations between defect rates become irrelevant, and the time scales of oscillations become robust to fluctuations in these irrelevant variables.

Our results give insight in to why biochemical oscillators might evolve to consume large amounts of energy in the form of ATP [15]. In addition to the previously known function of suppressing uncertainty in the period of the oscillator for a system with uniform rates [8, 17], it also makes the time scales of the oscillator more robust to fluctuations in the rates caused by the noisy environment of the cell.

One limitation of our results is that we restricted ourselves to a single cycle of states, representing the average path of a limit-cycle oscillator in a high-dimensional state space. We anticipate that our results can be extended to situations where the oscillator is allowed to fluctuate off of this average path. In Ref. [8], the authors argue that in a multicyclic network one cycle will dominate and that the bound on global oscillations will be limited by the affinity and number of states of the dominant cycle. Similarly, if the oscillator has a dominant cycle and multiple secondary cycles, we expect that our results can be applied by coarse-graining the secondary cycles to obtain effective rates and then using our expression in Eq. 3 for the main cycle. This extension will be explored in future work. Our theory, and its implications for the robustness of oscillator timescales, is therefore expected to be relevant to a broad class of networks with disordered rates and potentially many cycles.

ACKNOWLEDGEMENTS

We thank Robert Jack and Kabir Husain for helpful comments on an earlier version of this manuscript. CdJ acknowledges the support of the Natural Sciences and Engineering Research Council of Canada (NSERC). CdJ a été financée par le Conseil de recherches en sciences naturelles et en génie du Canada (CRSNG). This work was partially supported by the University of Chicago Materials Research Science and Engineering Center (MRSEC), which is funded by the National Science Foundation under award number DMR-1420709. SV also acknowledges support from the Sloan Fellowship and the University of Chicago.

-
- [1] C. H. Johnson, C. Zhao, Y. Xu, and T. Mori, *Nature Reviews Microbiology* **15**, 232 (2017).
- [2] S. Panda, J. B. Hogenesch, and S. A. Kay, *Nature* **417**, 329 (2002).
- [3] B. Novák and J. J. Tyson, *Nature Reviews Molecular Cell Biology* **9**, 981 (2008).
- [4] M. Nakajima, K. Imai, H. Ito, T. Nishiwaki, Y. Murayama, H. Iwasaki, T. Oyama, and T. Kondo, *Science* **308**, 414 (2005).
- [5] M. A. Woelfle, Y. Ouyang, K. Phanvijhitsiri, and C. H. Johnson, *Current Biology* **14**, 1481 (2004).
- [6] W. Pittayakanchit, Z. Lu, J. Chew, M. J. Rust, and A. Murugan, *eLife* **7** (2018), 10.7554/eLife.37624.
- [7] N. Barkai and S. Leibler, *Nature* **403**, 267 (2000).
- [8] A. C. Barato and U. Seifert, *Physical Review E* **95**, 062409 (2017).
- [9] A. C. Barato and U. Seifert, *Physical Review Letters* **114**, 158101 (2015).
- [10] T. R. Gingrich, J. M. Horowitz, N. Perunov, and J. L. England, *Physical Review Letters* **116**, 120601 (2016).
- [11] L. G. Morelli and F. Jülicher, *Physical Review Letters* **98**, 228101 (2007).
- [12] M. J. Rust, J. S. Markson, W. S. Lane, D. S. Fisher, and E. K. O’Shea, *Science* **318**, 809 (2007).
- [13] J. S. van Zon, D. K. Lubensky, P. R. H. Altena, and P. R. ten Wolde, *Proceedings of the National Academy of Sciences of the United States of America* **104**, 7420 (2007).
- [14] U. Seifert, *Rep. Prog. Phys.* **75**, 126001 (2012).
- [15] K. Terauchi, Y. Kitayama, T. Nishiwaki, K. Miwa, Y. Murayama, T. Oyama, and T. Kondo, *Proceedings of the National Academy of Sciences of the United States of America* **104**, 16377 (2007).
- [16] H. Qian and M. Qian, *Physical Review Letters* **84**, 2271 (2000).
- [17] Y. Cao, H. Wang, Q. Ouyang, and Y. Tu, *Nature Physics* **11**, 772 (2015).
- [18] B. Nguyen, U. Seifert, and A. C. Barato, *The Journal of Chemical Physics* **149**, 045101 (2018).
- [19] E. Leypunskiy, J. Lin, H. Yoo, U. Lee, A. R. Dinner, and M. J. Rust, *Elife* **6** (2017), 10.7554/eLife.23539.
- [20] J. J. Hopfield, *Proceedings of the National Academy of Sciences* **71**, 4135 (1974).
- [21] C. H. Bennett, *Biosystems* **11**, 85 (1979).
- [22] H. Qian, *Journal of Molecular Biology* **362**, 387 (2006).
- [23] G. Lan, P. Sartori, S. Neumann, V. Sourjik, and Y. Tu, *Nature Physics* **8**, 422 (2012).
- [24] P. Mehta and D. J. Schwab, *Proceedings of the National Academy of Sciences of the United States of America* **109**, 17978 (2012).
- [25] A. Murugan, D. A. Huse, and S. Leibler, *Proceedings of the National Academy of Sciences of the United States of America* **109**, 12034 (2012).
- [26] H. Wierenga, P. R. ten Wolde, and N. B. Becker, *Physical Review E* **97**, 042404 (2018).
- [27] See Supplemental Material at (URL will be inserted by publisher).
- [28] R. R. Aldrovandi, *Special matrices of mathematical physics : stochastic, circulant, and Bell matrices* (World Scientific, 2001) p. 323.
- [29] S. Vaikuntanathan, T. R. Gingrich, and P. L. Geissler, *Physical Review E* **89**, 062108 (2014).
- [30] A. Crisanti, G. Paladin, and A. Vulpiani, *Products of random matrices in statistical physics* (Springer, 1993) p. 166.
- [31] A. Amir, N. Hatano, and D. R. Nelson, *Physical Review E* **93**, 042310 (2016).
- [32] L. Onsager, *Physical Review* **65**, 117 (1944).
- [33] Technically one rate must be uniform or else Eq. 4 diverges. However, if only one rate is uniform, with extremely high probability no two rates in the network will be the same, so we call this a completely disordered network.
- [34] R. Milo and R. Phillips, *Cell biology by the numbers* (Garland Science, 2015).

Supplementary Material: High chemical affinity increases the robustness of biochemical oscillations

Clara del Junco and Suriyanarayanan Vaikuntanathan

Department of Chemistry and The James Franck Institute, University of Chicago, Chicago, IL, 60637

I. THE FIRST NON-ZERO EIGENVALUE AS AN APPROXIMATION OF THE NUMBER OF COHERENT OSCILLATIONS AND PERIOD OF OSCILLATIONS

In a system such as the one pictured in Fig. 1 of the main text, we can define correlation function $C_{11}(t)$ as the conditional probability of the system being in state 1 at time t given that it began in state 1 at time 0. It is given by the solution of the master equation:

$$C_{11}(t) \equiv [\exp(\mathbf{W}t)\mathbf{P}(0)]_1 \quad (1)$$

$$= \sum_{m=0}^{N-1} \frac{1}{N} e^{\phi_j t} \quad (2)$$

$$= \sum_{m=0}^{N-1} \exp[-\text{Re}[\phi_j]t](\cos[\text{Im}[\phi_j]t] + i \sin[\text{Im}[\phi_j]t]) \quad (3)$$

where ϕ_j are the N eigenvalues of the $N \times N$ matrix \mathbf{W} and $[\dots]_1$ is the first element of the vector.

To see why the first non-zero eigenvalue ϕ_1 , which we simply denote ϕ in the main text, is sufficient to approximate the number of coherent oscillations, we begin with the uniform case. As noted in the main text and illustrated in Fig. 1, the transition rate matrix \mathbf{W}_0 for this system is a circulant matrix whose eigenvalues lie in an ellipse in the complex plane with semi-major axis $a = k^+ + k^-$ and semi-minor axis $b = k^+ - k^-$ centered on the point $(-a, 0)$. When the affinity is large and $k^+/k^- \gg 1$, this effectively becomes a circle of radius $r = k^+$ centered at $(-r, 0)$.

The first eigenvalue is $\phi_0 = 0$, so the first term of the sum in Eq. 2 gives a constant contribution of $1/N$. The angle from the real axis to the j th eigenvalue ϕ_j is $2\pi j/N$. The imaginary part of ϕ_j is given by $r \sin(2\pi j/N)$, and the period of oscillations of the m th term in Eq. 3 is $T_j = 2\pi/(r \sin(2\pi j/N))$. The ratio of T_1 from the first non-zero eigenvalue to T_j from any subsequent eigenvalue is:

$$\frac{T_j}{T_1} = \frac{\sin(2\pi/N)}{\sin(2\pi j/N)} \approx \frac{2\pi/N}{2\pi j/N} = \frac{1}{j} \quad (4)$$

for $N \gg j$. The total period of the oscillations is therefore always T_1 . Since $\text{Re}[\phi_1] < \text{Re}[\phi_j]$ for all $j > 1$, the number of oscillations of the correlation function \mathcal{N} is given exactly by $|\text{Im}[\phi_1]|/(-2\pi \text{Re}[\phi_1]) = \mathcal{R}/2\pi$. Moreover, by the same reasoning the ratio of decay times τ_j/τ_1 where $\tau_i = -1/\text{Re}[\phi_i]$ is j^2 , so oscillations due to the second eigenvalue are damped out four times faster than the first, and the $j = 1$ term is the only important oscillating contribution to $C_{11}(t)$ for after a transient period.

When defects are added the eigenvalues will no longer lie on a perfect circle in the plane, and the arguments above will no longer hold exactly. For small perturbations (1 or 2 defect rates) it is reasonable to assume that the eigenvalues will not change very much and that $\mathcal{R}/2\pi \approx \mathcal{N}$. However, for large amounts of disorder it is not obvious that this will still be the case. T_j/T_1 may no longer be an integer, so that the total period of oscillations $T \neq T_1$, and moreover the period of the oscillations at short times ($T(1)$) and the period of oscillations at long times ($T(\tau)$) may not be the same. While $T(\tau)$ should be close to T_1 , since all other contributions will have been damped out, $T(1)$ may not be. Yet, if the oscillator needs to be tuned to have the same period as an external signal to which it is entrained, T_1 (or T_j where j is a small integer) is likely to be the most relevant timescale.

In Fig. 2 we show histograms of the relative difference $(T(1) - T_1)/T(1)$ for different realization of matrices of size $N = 100$ with reverse rates all equal to 1, random forward rates h_i^+ chosen from a Gaussian distribution with mean $\mu = \exp(\mathcal{A}/N)$ and variance $\sigma^2 = 0.25 \exp(\mathcal{A}/N)$, and uniform forward rates k^+ set to maintain a constant \mathcal{A} . We emphasize that here we are considering the difference between the first term of Eq. 2 and the full correlation function, both of which are obtained by numerical diagonalization. The theory presented in the main text is another level of approximation of T_1 on top of this.

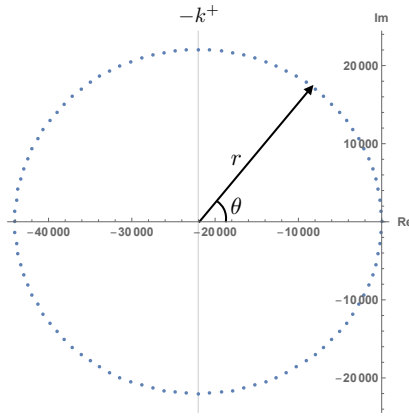


FIG. 1. Eigenvalues of a circulant matrix representing a network of size $N = 100$ with uniform rates $k^+ = e^{10}$ and $k^- = 1$.

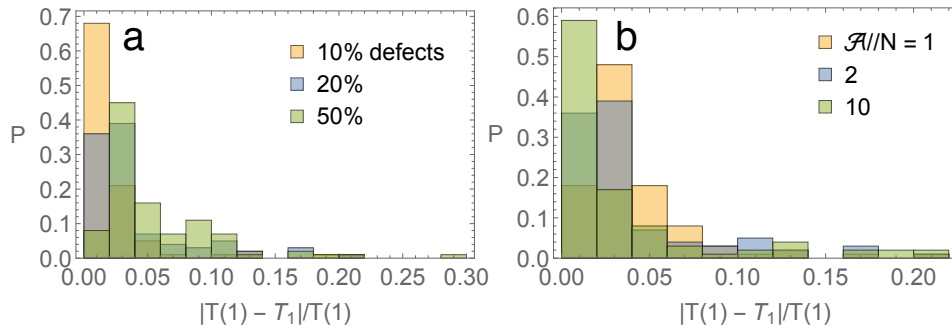


FIG. 2. Histograms of the relative difference between the first period of oscillations of the correlation function $C_{11}(t)$ ($T(1)$) and the period of oscillations due to the first eigenvalue $T_1 = 2\pi/\text{Im}[\phi]$. $T(1)$ is the location of the first peak of $C_{11}(t)$ obtained by exponentiating the full transition rate matrix. T_1 was calculated from the first eigenvalue, which was also obtained numerically. The data for each set of parameters were obtained from 100 randomly generated matrices (a) At constant $\mathcal{A}/N = 2$ The agreement between $T(1)$ and T_1 gets worse with increasing disorder. (b) With the percent of defects held constant at 20%, the agreement between $T(1)$ and T_1 improves with increasing \mathcal{A}/N .

II. DETAILED CALCULATIONS

A. Transfer matrix formulation

To find the first non-zero eigenvalue ϕ of the transition matrix \mathbf{W} in the disordered system, we will take advantage of the local nature of connections in this system to recast the eigenvalue problem in terms of transfer matrices.

Consider the eigenvalue equation for the circulant matrix \mathbf{W}_0 :

$$\begin{bmatrix} -(k^- + k^+) & k^- & \dots & k^+ \\ k^+ & -(k^- + k^+) & k^- & \dots \\ \vdots & & \ddots & \\ k^- & \dots & k^+ & -(k^- + k^+) \end{bmatrix} \begin{bmatrix} f_1 \\ f_2 \\ \vdots \\ f_N \end{bmatrix} = \phi^{(0)} \begin{bmatrix} f_1 \\ f_2 \\ \vdots \\ f_N \end{bmatrix} \quad (5)$$

We can then write:

$$-(k^- + k^+)f_1 + k^- f_2 + k^+ f_N = \phi^{(0)} f_1 \quad (6)$$

$$-(k^- + k^+)f_2 + k^- f_3 + k^+ f_1 = \phi^{(0)} f_2 \quad (7)$$

and so forth, with

$$\phi^{(0)} = -(k^- + k^+) + k^- \exp(-2\pi i/N) + k^+ \exp(2\pi i/N). \quad (8)$$

Solving for f_1 in Eq. 7 gives:

$$f_1 = \frac{\phi^{(0)} + k^- + k^+}{k^+} f_2 - \frac{k^-}{k^+} f_3 \quad (9)$$

which we can also write as:

$$\begin{bmatrix} f_1 \\ f_2 \end{bmatrix} = \begin{bmatrix} \frac{\phi^{(0)} + k^- + k^+}{k^+} & -\frac{k^-}{k^+} \\ 1 & 0 \end{bmatrix} \begin{bmatrix} f_2 \\ f_3 \end{bmatrix} \equiv \mathbf{B} \begin{bmatrix} f_2 \\ f_3 \end{bmatrix}. \quad (10)$$

Thus, \mathbf{B} maps the eigenvector magnitudes (f_{i-1}, f_i) to (f_i, f_{i+1}) . Because the matrix \mathbf{B} is the same for each link in the unicyclic network with uniform rates, we have:

$$\begin{bmatrix} f_1 \\ f_2 \end{bmatrix} = \mathbf{B}^N \begin{bmatrix} f_1 \\ f_2 \end{bmatrix} \quad (11)$$

so that \mathbf{B}^N must have an eigenvalue of 1. Solving for the eigenvalues of \mathbf{B}^N will give a polynomial of order $(\phi^{(0)})^N$, the N roots of which are the N eigenvalues of the transition matrix \mathbf{W}_0 . This gives us an alternative to Eq. 5 for finding $\phi^{(0)}$.

B. One defect rate

We first consider the case of adding one set of “defect” rates h^\pm . To do so we replace one of the \mathbf{B} matrices in the product in Eq. 11 by

$$\mathbf{A} \equiv \begin{bmatrix} \frac{\phi + h^- + h^+}{h^+} & -\frac{h^-}{h^+} \\ 1 & 0 \end{bmatrix}. \quad (12)$$

which maps the eigenvector elements on either side of the link with the defect rates. The new product of transfer matrices is:

$$\begin{bmatrix} f_1 \\ f_2 \end{bmatrix} = \mathbf{A} \mathbf{B}^{N-1} \begin{bmatrix} f_1 \\ f_2 \end{bmatrix}. \quad (13)$$

Now the \mathbf{B} matrix has changed, since modifying the rates changes the value of ϕ . We write ϕ in the most general way as:

$$\phi = \phi^{(0)} + C\gamma \quad (14)$$

where C is a constant to be determined, which implies

$$\mathbf{B} = \mathbf{B}_0 + \begin{bmatrix} C\gamma/(k^+) & 0 \\ 0 & 0 \end{bmatrix} \equiv \mathbf{B}_0 + \mathbf{B}_1 \quad (15)$$

with \mathbf{B}_0 given by equation 10.

We now proceed with the matrix perturbation of \mathbf{B} . First we compute the eigenvalues (β_i) and normalized eigenvectors of \mathbf{B}_0 . Note that since \mathbf{B}_0 is non-Hermitian, its right and left eigenvectors ($|i\rangle$ and $\langle i|$) are not the same and we need to compute them separately in order to get an orthonormal basis set [1]. The left eigenvectors of \mathbf{B}_0 are the right eigenvectors of \mathbf{B}_0^\dagger (the conjugate transpose of \mathbf{B}_0). We obtain:

$$\beta_1^0 = e^{2\pi i/N} \quad \beta_2^0 = (k^-/k^+)e^{-2\pi i/N} \quad (16)$$

$$|1_0\rangle = \frac{1}{c_1}(e^{2\pi i/N}, 1) \quad |2_0\rangle = \frac{1}{c_2}((k^-/k^+)e^{-2\pi i/N}, 1) \quad (17)$$

$$\langle 1_0| = \frac{1}{c_1}(-(k^+/k^-)e^{2\pi i/N}, 1) \quad \langle 2_0| = \frac{1}{c_2}(-e^{-2\pi i/N}, 1) \quad (18)$$

$$c_1^2 = 1 - (k^+/k^-)e^{4\pi i/N} \quad c_2^2 = 1 - (k^-/k^+)e^{-4\pi i/N} \quad (19)$$

(it is easy to verify that this is an orthonormal basis set). Now we compute the first-order correction to the eigenvalues:

$$\beta_1^{(1)} = \langle 1_0|\mathbf{B}_1|1_0\rangle = -\frac{e^{4\pi i/N} C\gamma}{c_1^2 k^-}. \quad (20)$$

We choose

$$C = c_1^2 k^- e^{-2\pi i/N} \quad (21)$$

so that

$$\beta_1^{(1)} = e^{2\pi i/N} \gamma \quad (22)$$

giving

$$\beta_1 = e^{2\pi i/N} (1 + \gamma). \quad (23)$$

Similarly,

$$\beta_2 = \frac{k^-}{k^+} e^{-2\pi i/N} (1 + \gamma) = e^{-\mathcal{A}/N} e^{-2\pi i/N} (1 + \gamma). \quad (24)$$

We can now compute \mathbf{B}^{N-1} using:

$$\mathbf{B}^{N-1} = \sum_i \beta_i^{N-1} \mathbf{X}_i^0 \quad (25)$$

where $\mathbf{X}_i^0 \equiv |i_0\rangle \langle i_0|$ is the outer product of zero-order eigenvectors. Since $\beta_2 \propto e^{-\mathcal{A}/N} < 1$, we can see that if \mathcal{A} is sufficiently large, all of the terms containing β_2 will vanish. Then, Eq. 13 reduces to:

$$\begin{bmatrix} f_1 \\ f_2 \end{bmatrix} = \beta_1^{N-1} \mathbf{A} \mathbf{X}_1^{(0)} \begin{bmatrix} f_1 \\ f_2 \end{bmatrix} \quad (26)$$

where $\mathbf{X}_1^{(0)}$ is:

$$\mathbf{X}_1^{(0)} = \frac{1}{c_1^2} \begin{bmatrix} -e^{4\pi i/N} k^+ / k^- & e^{2\pi i/N} \\ -e^{2\pi i/N} k^+ / k^- & 1 \end{bmatrix} \quad (27)$$

1. Comparing to exact eigenvalues of \mathbf{B}

Since \mathbf{B} is a two by two matrix, we can compute its exact eigenvalues and check how the error in our perturbative approximations of β_1 and β_2 scales. This will reveal what the ‘perturbative parameter’ in our theory is. The exact eigenvalues of \mathbf{B} are:

$$\beta_{\text{exact}}^{\pm} = \frac{e^{-2\pi i/N}}{2} \left(\frac{k^-}{k^+} (1 - \gamma) + e^{4\pi i/N} (1 + \gamma) \pm \left[-4e^{4\pi i/N} \frac{k^-}{k^+} + \left(\frac{k^-}{k^+} (1 - \gamma) + e^{4\pi i/N} (1 + \gamma) \right)^2 \right]^{1/2} \right) \quad (28)$$

$$= \frac{e^{-2\pi i/N}}{2} \left(e^{-\mathcal{A}/N} (1 - \gamma) + e^{4\pi i/N} (1 + \gamma) \pm \left[-4e^{4\pi i/N} e^{-\mathcal{A}/N} + \left(e^{-\mathcal{A}/N} (1 - \gamma) + e^{4\pi i/N} (1 + \gamma) \right)^2 \right]^{1/2} \right) \quad (29)$$

If we ignore terms of order $e^{-\mathcal{A}/N}$ compared to terms of order 1, the expressions above simplify to:

$$\lim_{\exp(-\mathcal{A}/N) \rightarrow 0} \beta_{\text{exact}}^{\pm} = \frac{e^{2\pi i/N}}{2} ((1 + \gamma) \pm (1 + \gamma)) \quad (30)$$

giving

$$\lim_{\exp(-\mathcal{A}/N) \rightarrow 0} \beta_{\text{exact}}^+ = e^{2\pi i/N} (1 + \gamma) = \beta_1 \quad \lim_{\exp(-\mathcal{A}/N) \rightarrow 0} \beta_{\text{exact}}^- = 0 \quad (31)$$

In the limit of very high affinity, Eq. 26 is exact. Therefore, the small parameter in our theory is $\exp(\mathcal{A}/N)$.

2. Solving for γ

We can now compute the matrix product in Eq. 26 and set its eigenvalue equal to 1 in order to solve for ϕ . Recall that \mathbf{A} is also a function of ϕ , so we will also include γ in \mathbf{A} . In the case of a single defect, where γ is small, this effect is likely to be insignificant and it would be sufficient to approximate \mathbf{A} as a function of $\phi^{(0)}$ only. However, below we will add multiple defects to the network and in that case, including γ in \mathbf{A} is important. We find:

$$\mathbf{A}\mathbf{X}_1^{(0)} \equiv \mathbf{Z} = \frac{1}{c_1^2} \begin{bmatrix} da & db \\ a & b \end{bmatrix} \quad (32)$$

where

$$d(h^\pm) = \frac{\gamma + e^{-2i\pi/N}(k^- - h^-) + k^+ e^{2i\pi/N} + h^- + h^+ - k^- - k^+}{h^+} \quad (33)$$

$$a = -e^{4\pi i/N} k^+ / k^- \quad (34)$$

$$b = e^{2\pi i/N} \quad (35)$$

Since the two rows of \mathbf{Z} are related by a constant, \mathbf{Z} has a zero eigenvalue. The non-trivial eigenvalue ζ of \mathbf{Z} is:

$$\zeta = \frac{e^{2\pi i/N} \left(k^+ e^{2\pi i/N} (-C\gamma - h^- - h^+ + k^- + k^+) + h^- k^+ + h^+ k^- - k^- k^+ - e^{4\pi i/N} k^{+2} \right)}{c_1^2 h^+ k^-}. \quad (36)$$

We can now solve for γ using:

$$1 = \beta_1^{N-1} \zeta \quad (37)$$

$$= e^{-2\pi i/N} (1 + \gamma)^{N-1} \zeta \quad (38)$$

For notational simplicity we absorb the $e^{-2\pi i/N}$ term in to ζ , letting

$$\zeta' = e^{-2\pi i/N} \zeta. \quad (39)$$

Rearranging, we have:

$$(1 + \gamma) = \zeta'^{1/(1-N)} \quad (40)$$

We now rewrite $\zeta'^{1/(1-N)}$ as $\exp(\log(\zeta'^{1/(1-N)})) = \exp\left(\left(\frac{1}{1-N}\right) \log(\zeta')\right)$ and expand:

$$\exp\left(\left(\frac{1}{1-N}\right) \log(\zeta')\right) \approx 1 + \frac{1}{1-N} \log(\zeta') + \frac{1}{2(1-N)^2} (\log(\zeta'))^2 + \dots, \quad (41)$$

giving

$$1 + \gamma \approx 1 + \frac{1}{1-N} \log(\zeta') + \frac{1}{2(1-N)^2} (\log(\zeta'))^2 \quad (42)$$

The 1's cancel and we get:

$$\gamma \approx \frac{1}{1-N} \log(\zeta') + \frac{1}{2(1-N)^2} (\log(\zeta'))^2. \quad (43)$$

This gives a self-consistent equation for γ (since ζ' is a function of γ). To obtain the results in the main text, we solved eq. 43 numerically by searching for roots of the equation in the neighborhood of the analytical approximation that we can obtain from expanding the logarithms in eq. 43 to first order. To obtain this analytical approximation we rewrite ζ' as:

$$\zeta' = \zeta'_0 - \gamma \frac{k^+ e^{2\pi i/N} C}{c_1^2 h^+ k^-} = \zeta'_0 - \gamma \frac{k^+}{h^+} \quad (44)$$

where ζ'_0 is independent of γ . We then expand the logarithm as:

$$\log(\zeta') = \log\left(\zeta'_0 - \gamma \frac{k^+}{h^+}\right) \quad (45)$$

$$= \log\left(\zeta'_0 \left(1 - \gamma \frac{k^+}{h^+ \zeta'_0}\right)\right) \quad (46)$$

$$\approx \log(\zeta'_0) - \gamma \frac{k^+}{h^+ \zeta'_0} \quad (47)$$

where in the last line we have used $\log(1+x) \approx x$ for $x \ll 1$. Plugging this back in to Eq. 43 and keeping only the term linear in $1/(1-N)$ gives:

$$\gamma \approx \frac{1}{1-N} \log(\zeta'_0) - \gamma \frac{k^+}{h^+ \zeta'_0}. \quad (48)$$

C. Many Defect Rates

Now we extend our results to the case where many (m) of the rates are ‘defects’. The product of transfer matrices in this case is:

$$\begin{bmatrix} f_1 \\ f_2 \end{bmatrix} = \mathbf{A}_1 \mathbf{B}^{L_1} \dots \mathbf{A}_j \mathbf{B}^{L_j} \dots \mathbf{A}_m \mathbf{B}^{L_m} \begin{bmatrix} f_1 \\ f_2 \end{bmatrix}. \quad (49)$$

where L_j is the distance between neighboring defect rates and $\sum_j L_j = N - m$.

1. Defect spacing $L_j \geq 1$

Recall that

$$\mathbf{B}^{L_j} = \left(e^{-2\pi i/N} (1 + \gamma)\right)^{L_j} \mathbf{X}_1^0 + \left(e^{-A/N} e^{-2\pi i/N} (1 + \gamma)\right)^{L_j} \mathbf{X}_2^0. \quad (50)$$

Generally, this means that eq. 49 has 2^m terms. However, if $e^{-L_j A/N}$ is sufficiently large, we can ignore β_2 as we did in the case of one defect above. Then, eq. 49 reduces to a single term from which we can factorize β_1 , giving:

$$\begin{bmatrix} f_1 \\ f_2 \end{bmatrix} = \beta_1^{N-m} \mathbf{A}_1 \mathbf{X}_1^{(0)} \dots \mathbf{A}_j \mathbf{X}_1^{(0)} \dots \mathbf{A}_m \mathbf{X}_1^{(0)} \begin{bmatrix} f_1 \\ f_2 \end{bmatrix} \quad (51)$$

The affinity thus sets a correlation length for the defects; if the affinity per site (A/N) is sufficiently large, the spacing between them does not matter. In principle, the order of the matrices in the matrix product in Eq. 51 is however still important and hence the values of ϕ and \mathcal{R} depend on the order of the defects. However, our calculations are simplified due to the special symmetry of $\mathbf{Z}_j \equiv \mathbf{A}_j \mathbf{X}_1^{(0)}$ (given explicitly by Eq. 32 with the defect rates h^\pm now indexed h_j^\pm , etc.). It turns out that the non-trivial eigenvalue of the product $\mathbf{Z}_i \mathbf{Z}_j$ is the product of the non-trivial eigenvalues of \mathbf{Z}_i and \mathbf{Z}_j . As a result, the expression for ϕ is simply determined by the product of the non-trivial eigenvalues of the \mathbf{Z}_j matrices. Therefore, as long as $L_j \geq 1 \forall j$, the order in which the defects are placed and the spacing between them becomes irrelevant as far as ϕ is concerned. We can simply extend our results for one defect to write:

$$\gamma \approx \frac{1}{m-N} \sum_{j=1}^m \log(\zeta'_j) + \frac{1}{2(m-N)^2} (\log(\zeta'_j))^2. \quad (52)$$

where ζ'_j is a function of $k^+, k^-, h_j^+, h_j^-, N$ given by eq. 36 and 39 but is independent of any of the other defect rates. The corresponding analytical approximation is:

$$\gamma \approx \frac{1}{1-N} \sum_{j=1}^m \log(\zeta'_{0,j}) - \gamma \frac{k^+}{h^+ \sum_{j=1}^m \zeta'_{0,j}}. \quad (53)$$

Our derivation depends on the distance between defect rates in the networks being at least one ($L_j \geq 1$). Nonetheless, our numerical results in the main text show that these expressions accurately predict the eigenvalues of the oscillator even when $L_j = 0$ for nearly all of the defects. We now discuss how high affinity makes this possible.

2. Defect spacing $L_j = 0$

The reason we require $L_j \geq 1$ is that the non-trivial eigenvalue of the product $\mathbf{Z}_i \mathbf{Z}_j$, where $\mathbf{Z}_j \equiv \mathbf{A}_j \mathbf{X}_1^{(0)}$, is the product of the non-trivial eigenvalues of \mathbf{Z}_i and \mathbf{Z}_j . However, the eigenvalue of the product of $\mathbf{A}_i \mathbf{A}_j$ is *not* the product of their eigenvalues. Therefore, Eq. 52 should not be valid if there are defect rates on either side of the same node in the network. In this case we need to consider the products $\mathbf{A}_i \mathbf{A}_j$, $\mathbf{A}_i \mathbf{A}_j \mathbf{A}_k$, etc., for clusters of 2, 3, etc. defects. We find that the matrices

$$\mathbf{Z}_2^{ij} \equiv \mathbf{A}_j \mathbf{A}_i \mathbf{X}_1^{(0)} \quad (54)$$

$$\mathbf{Z}_3^{ijk} \equiv \mathbf{A}_j \mathbf{A}_i \mathbf{A}_k \mathbf{X}_1^{(0)} \quad (55)$$

$$\dots \quad (56)$$

$$\mathbf{Z}_m^{ij\dots} \equiv \mathbf{A}_j \mathbf{A}_i \dots \mathbf{A}_m \mathbf{X}_1^{(0)} \quad (57)$$

have the same properties as the \mathbf{Z} matrices, i.e. the eigenvalue of the product $\prod \mathbf{Z}_m^{ij\dots} \mathbf{Z}_n^{kl\dots}$ is the product of the eigenvalues of $\mathbf{Z}_{m,ij\dots m}$ and $\mathbf{Z}_{n,kl\dots n}$. Clearly there is a way of including higher and higher order correlations, but as soon as we include *any* coupling of the defects we need a lot more information about their positions. In order for the defects to be completely decoupled from one another, as indeed we find that they are even at moderate affinities $\mathcal{A}/N \approx 2$, we need the eigenvalue of the product of $\mathbf{A}_i \mathbf{A}_j$ to be the product of their eigenvalues. Let us write \mathbf{A}_j as

$$\mathbf{A}_j = \begin{bmatrix} x_j & -y_j \\ 1 & 0 \end{bmatrix} \quad (58)$$

where

$$x_j = \frac{\phi + h_j^- + h_j^+}{h_j^+} = \frac{h_j^- e^{-2\pi i/N} + h_j^+ e^{-2\pi i/N} + C\gamma/N}{h_j^+} \quad y_j = \frac{h_j^-}{h_j^+} \quad (59)$$

In the limit of large N , we have:

$$\lim_{N \rightarrow \infty} x_j = \frac{h_j^- + h_j^+}{h_j^+} = 1 + \frac{h_j^-}{h_j^+} \quad y_j = \frac{h_j^-}{h_j^+}. \quad (60)$$

The eigenvalues of \mathbf{A}_j are

$$\alpha_1^j = \frac{1}{2} \left(\sqrt{x_j^2 + 4y_j} + x_j \right), \alpha_2^j = 0. \quad (61)$$

The eigenvalues of the product $\mathbf{A}_j \mathbf{A}_i$ are:

$$\alpha_1^{ij} = \frac{1}{2} \left(-\sqrt{(x_i x_j + y_i + y_j)^2 - 4y_i y_j} + x_i x_j + y_i + y_j \right) \quad (62)$$

$$\alpha_2^{ij} = \frac{1}{2} \left(\sqrt{(x_i x_j + y_i + y_j)^2 - 4y_i y_j} + x_i x_j + y_i + y_j \right) \quad (63)$$

If we can ignore the y terms compared to the x terms, then these reduce to:

$$\lim_{y/x \rightarrow 0} \alpha_1^{ij} = 0 \quad (64)$$

$$\lim_{y/x \rightarrow 0} \alpha_2^{ij} = x_i x_j \quad (65)$$

and the eigenvalues of \mathbf{A}_i become $\alpha_1^i = x_i, \alpha_2^i = 0$. Clearly, in this limit the eigenvalue of the product of transfer matrices is equal to the product of eigenvalues, as required, and the order of the defects will no longer matter even if they are adjacent. The limit is fulfilled when the affinity is high so that $h^-/h^+ \sim \exp(-\mathcal{A}/N)$.

Following the derivation above using x_j as the eigenvalue for the defect transfer matrices, we obtain the same result as in eqs. 52 and 53 with ζ replaced by x . Indeed, we see that in the limit that $h^-/h^+ \rightarrow 0$ and $k^-/k^+ \rightarrow 0$, ζ reduces to x . This explains how our theory can handle many adjacent defects.

III. CONSTANT AFFINITY RESULTS

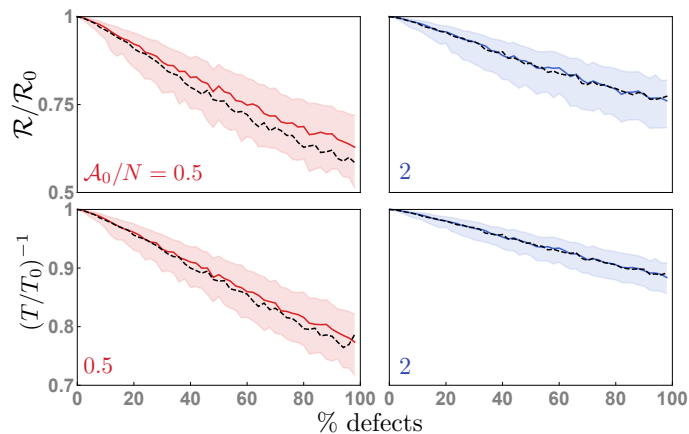


FIG. 3. Coherence \mathcal{R} and period T of an oscillator with $N = 100$ states as a function of the percent of defect rates. All counterclockwise rates are set to 1. We restrict ourselves to even numbers of defect rates. Half of the clockwise defect rates $\{h_j^+\}$ are drawn from a Gaussian distribution with mean $k^+ = \exp(\mathcal{A}_0/N)$ and standard deviation $0.4k^+$, and with a lower cutoff at 0.1 so that we do not select rates that are very close to zero or negative. We set the other half of the defect rates to $\{\exp(\mathcal{A}_0/N)^2/h_j^+\}$. This prescription ensures that the affinity remains constant and equal to \mathcal{A}_0 , while also allowing the rates to vary over at least an order of magnitude. Red curves are for $\mathcal{A}_0/N = 0.5$; blue curves $\mathcal{A}_0/N = 2$. Because the distributions of \mathcal{R} and T are asymmetric, rather than plotting the mean and standard deviation of the data we plot the median (solid line) \pm one quartile (shaded region) of the numerical values for 500 samples of defect rates. The dashed lines are the median theoretical predictions for 500 samples of defect rates. Our results confirm the bound in Ref. [2], as the value of $\mathcal{R}/\mathcal{R}_0$ is never greater than 1. For $\mathcal{A}_0/N = 2$, our theory is accurate even when % defects ≈ 100 . Our results confirm the bound in Ref. [2], as the value of $\mathcal{R}/\mathcal{R}_0$ is never greater than 1, and show that \mathcal{R} and T become more robust (spread of values decreases) and predictable at high affinity.

-
- [1] R. A. Marcus, J. Phys. Chem. A **105**, 2612 (2001).
 [2] A. C. Barato and U. Seifert, Phys. Rev. E **95**, 062409 (2017).